


New measurement of residues from ${}^7\text{Li} + {}^{\text{nat}}\text{Ta}$ reaction within 4–6.5 MeV/nucleon: Production yield for ${}^{183}\text{Os}$

Amit Chauhan and Moumita Maiti*

Department of Physics, Indian Institute of Technology Roorkee, Roorkee 247667, Uttarakhand, India
 (Received 5 September 2018; revised manuscript received 19 December 2018; published 11 March 2019)

Exploration of reaction dynamics of the weakly bound heavy-ion interaction with an intermediate or heavy mass target in the low energy range has been a subject of interest over the past decades; however, different modes of fusion such as breakup fusion, incomplete fusion, and transfer phenomena observed experimentally are not yet fully understood. Experimental studies are therefore essential to address the problem. In this article, we report a new set of cross-section data of the residues produced in the weakly bound ${}^7\text{Li}$ induced reaction on ${}^{\text{nat}}\text{Ta}$ within the 27–45 MeV energy range. Along with the major yield of ${}^{183\text{g+m}}\text{Os}$, production of ${}^{180\text{m}}\text{Hf}$ and ${}^{183}\text{Ta}$ are also observed up to ~ 35 MeV, which is possibly an indication of the incomplete fusion mechanism or breakup-transfer phenomena. The trend of the isomeric cross-section ratio of ${}^{183}\text{Os}$ indicates the role of angular momentum and spin distribution besides the excitation energy, and is interpreted by theory. The optimized production parameters and yields of ${}^{183\text{g,m}}\text{Os}$ are assessed.

DOI: [10.1103/PhysRevC.99.034608](https://doi.org/10.1103/PhysRevC.99.034608)

I. INTRODUCTION

Exploration of heavy-ion fusion is required to understand the dynamics of an excited composite nucleus approaching equilibrium and the mechanism of compound nucleus formation, as the multinucleon interaction in the fusion of heavy ions is complex in nature. Therefore, both theoretical and experimental studies of the formation and decay of the compound nucleus at low energy are important to understand the facts governing those reactions, and also the mechanism considered in the reaction models, to address some unsolved astrophysical problems, such as big-bang nucleosynthesis.

To understand the influence of weakly bound heavy projectiles (${}^{6,7}\text{Li}$, ${}^{9}\text{Be}$, etc.) in low energy reactions, several experiments have been carried out so far [1–16]. In fact, the study of heavy-ion induced reactions in medium and heavy targets is a tool to understand the threshold anomaly around the barrier, breakup fusion, preequilibrium processes, quasielastic effects, direct effects, transfer reactions, the role of cluster structure, etc. [17–33]. The interaction mechanism applies in weakly bound stable nuclei (${}^{6,7}\text{Li}$, ${}^9\text{Be}$), and radioactive projectiles are believed to be qualitatively the same, but the intensities of stable beams are several orders of magnitude larger than those presently available for radioactive beams. Thus, nuclear reactions induced by stable weakly bound nuclei are preferred.

Unlike tightly bound projectiles, direct breakup/transfer followed by fusion is observed for lightly bound projectiles. Reviews by Keeley *et al.* and Canto *et al.* [7,8,34,35] have described the influence of some important processes such as

elastic scattering, breakup reaction, and the dominant role of coupling to the breakup channel in the low energy fusion of weakly bound nuclei. Since the direct measurement of breakup cross sections is a hard task, most of the experiments determined fusion and elastic cross sections. The knowledge of fusion and breakup processes is directly relevant to producing nuclei near the drip line and possibly the synthesis of superheavy nuclei. The influence of partial fusion or incomplete fusion (ICF) of the weakly bound projectiles in the cases of ${}^6\text{Li} + {}^{208}\text{Pb}$ and ${}^9\text{Be} + {}^{209}\text{Bi}$ at energies above the Coulomb barrier and for the systems ${}^{6,7}\text{Li} + {}^{64}\text{Zn}$ and ${}^9\text{Be} + {}^{64}\text{Zn}$ near and above the Coulomb barrier have been studied by Liu *et al.* and Gomes *et al.*, respectively [36,37]. Complete fusion (CF) and ICF were also studied for the ${}^9\text{Be} + {}^{181}\text{Ta}$ reaction [38]. Parker *et al.* has explored the coupling effects of breakup and transfer reaction in ${}^9\text{Be}$ induced reactions on ${}^{28}\text{Si}$, ${}^{64}\text{Zn}$, and ${}^{144}\text{Sm}$ [39]. Capurro *et al.* has reported inelastic excitation in the ${}^{12}\text{C} + {}^{110,108}\text{Pd}$ reaction at sub-barrier energies (~ 3 – 4.5 MeV/A) and presence of transfer channels along with inelastic excitation in ${}^7\text{Li} + {}^{115,113}\text{In}$ at energies just above the barrier (~ 2.9 – 5.3 MeV/A) [40]. The available reports at sub-barrier energies show that the direct breakup of stable weakly bound nuclei dominates the transfer processes followed by a breakup [41]. Our group also has reported theoretical and experimental studies for ${}^7\text{Li}$, ${}^9\text{Be}$, and ${}^{12}\text{C}$ induced reactions on medium and heavy targets [20,21,42–46] within ~ 3.5 – 7 MeV/A energy range.

Further, in view of the growing demand of the neutron-deficient radionuclides of noble elements in applications, precise optimization of their production parameters is required. Although light-ion induced reactions are preferred to achieve better yield of the product radionuclide compared to the heavy-ion reactions, light heavy-ion reactions could be used to produce sufficient activity to conduct laboratory experiments.

*Corresponding author: moumifph@iitr.ac.in, moumifph@gmail.com

Thus the aim of this study is twofold: (1) to explore the production of ^{183}Os that may have possible application in diagnostic medicine and (2) to understand the fusion mechanism in the $^7\text{Li} + ^{\text{nat}}\text{Ta}$ reaction at low energies.

The physicochemical properties of ^{183}Os show its potential for medical application, and it can be produced in the no-carrier-added state. ^{183}Os has a half-life ($T_{1/2}$) of 13.0 h, it decays through electron capture (EC), and emits low energy γ rays of 114.43 keV (21.1%) and 381.74 keV (91.6%). The isomer $^{183\text{m}}\text{Os}$ ($T_{1/2} = 9.9$ h) decays through isomeric transition (IT, 15%) and EC (85%) followed by the emission of high energy γ rays 1101.94 keV (49%) and 1107.92 keV (22.3%), which may also be suitable in some specific cases. Due to the moderate half-life and low energy γ peaks of $^{183\text{g}}\text{Os}$, it is also a good choice for radiotracer studies. Finally, $^{183\text{m.g}}\text{Os}$ decays to long-lived ^{183}Re ($T_{1/2} = 70.0$ d), which is also favored for trace/ultra-trace scale geochemical research [47].

Considering these aspects, we have explored ^7Li induced reactions on $^{\text{nat}}\text{Ta}$ (0.012% $^{180}\text{Ta} + 99.988\%$ ^{181}Ta) within 27–45 MeV to understand the reaction mechanism involved in the low energy range. The measured cross sections are analyzed by comparing with the theoretical model calculations from ALICE14, EMPIRE3.2.2, and PACE4.

Ismail *et al.* [48] in late 1990s first reported the cross sections of $^{183\text{g.m}}\text{Os}$ from the $^7\text{Li} + ^{181}\text{Ta}$ reaction at four different energies and analyzed them by comparing with the ALICE91 code estimation. We performed extensive statistical model calculations and observed large deviations with the data of Ref. [48]. A second measurement of the residual cross section is, therefore, necessary to understand the reaction mechanism of $^7\text{Li} + ^{\text{nat}}\text{Ta}$ system and to estimate precisely the production yield of the residues.

The experimental procedure and a comparative study of the nuclear model calculations are presented in Sec. II. Section III discusses the details of theoretical calculations used in the present study, Sec. IV presents the results, and Sec. V summarizes the paper.

II. EXPERIMENTAL DETAILS

The experiment was performed at the BARC-TIFR Pelletron facility at TIFR, Mumbai, India. Natural tantalum (Ta) and aluminium (Al) foils, procured from Alfa Aesar, were rolled to produce self-supporting thin foils of Ta, having thickness of 1.8–3.3 mg/cm², and Al foils of 2–2.3 mg/cm². These foils were mounted on Al rings having 12 mm inner and 22 mm outer diameters. A target stack prepared by placing three Ta foils, each of which was backed by an Al foil, was irradiated with the $^7\text{Li}^{3+}$ beam having energy between 27 and 45 MeV, and five such target stacks were used in our experiment. The purpose of Al backing was to bring down the projectile energy and to trap the recoil residues in the forward stream of the beam. Assuming beam intensity to be almost constant, the degradation in incident beam energy through each successive foil is estimated by SRIM [49]. An electron-suppressed Faraday cup was placed to collect the total charge of each irradiation at the back side of the target assembly. The duration of irradiation was decided according to the beam

intensity and half-lives of the evaporation residues expected to be produced.

After the end of bombardment (EOB), the activity produced in each Ta-Al combination was measured with the help of γ -ray spectrometry using a high-purity germanium (HPGe) detector in a fixed geometry. The energy and efficiency calibration of the detector was done using a standard ^{152}Eu source of known strength. The energy resolution of the detector was 2.0 keV at 1332 keV. In the experimental geometry, efficiency was 10% at 121 keV and 2% at 1408 keV peak energy of ^{152}Eu . Multiple measurements were done for each Ta-Al combination to evaluate precisely the decay profile of the radionuclides produced in the Ta target.

The yield Y_r of an r th evaporation residue after the EOB is calculated using

$$Y_r = C(E_r) e^{\lambda_r t_c} \varepsilon_\gamma^{-1} I_\gamma^{-1}. \quad (1)$$

The cross section of the evaporation residue $\sigma_r(E)$ at an incident energy E is given by

$$\sigma_r(E) = \frac{\lambda_r Y_r}{I_b \rho_f t_f (1 - e^{-\lambda_r t_m})(1 - e^{-\lambda_r t_i})}, \quad (2)$$

where $C(E_r)$ is the net count under the photopeak area; ε_γ and I_γ are the detection efficiency of HPGe detector and branching intensity of the characteristic γ ray, respectively, of the evaporation residue. ρ_f is the number of nuclei per unit volume of the target foil; t_f is the thickness of target foil; λ_r is the decay constant; I_b is the beam intensity of the projectile; t_i , t_c , and t_m are the irradiation, cooling, and counting times, respectively [50]. The nuclear spectroscopic data used in the cross-section calculation of the evaporation residues are listed in Table I. The total uncertainty in the cross-section measurement is estimated from the following sources: (i) the inaccuracy in efficiency calibration of the detector ($\sim 1\%$), (ii) nonuniform thickness of the foil samples ($\sim 2\text{--}3\%$), (iii) inaccuracy in the current measurement of the $^7\text{Li}^{3+}$ beam ($\sim 6\text{--}7\%$), and (iv) statistical error in counting the γ rays ($\sim 1\text{--}2\%$). The errors due to the loss of beam energy in different foils and the branching ratio of characteristic γ rays have been assumed to be negligible in the present work.

III. THEORETICAL CALCULATION

A. PACE4

The statistical code PACE4 [51] is based on the Hauser-Feshbach (HF) formalism, which takes advantage of the Monte Carlo procedure using the framework of LISE++ [52]. The Monte Carlo calculation correlates γ rays and angular distribution of particles. For a heavy projectile, the Bass model is used to estimate the input fusion cross section of the evaporation residues. The Gilbert-Cameron (GC) level density is accounted for with level density parameter $a = A/9$ MeV⁻¹, where A is the mass number of the compound nucleus. The ratio a_f/a_n is assumed as unity. This code was used on a large number of events to acquire better statistics for the energy and angular distribution of residual nuclei. The transmission coefficient for light particles is determined during the first stage by optical model calculations and in subsequent phases by extrapolation from the initial steps. The

TABLE I. Spectroscopic data of the evaporation residues.

| Nuclide (J^π) | Half-life | Decay mode (%) | $E\gamma$ (keV) [$I\gamma$ (%)] | Reaction | E_{th}^a (MeV) |
|----------------------------------|-----------|------------------------------|---|--|------------------|
| ${}^{183g}\text{Os}$ ($9/2^+$) | 13.0 h | EC ^b (100) | 114.43 [21.1] 381.74 [91.6] | ${}^{181}\text{Ta}({}^7\text{Li}, 5n)$ | 31.4 |
| ${}^{183m}\text{Os}$ ($1/2^-$) | 9.9 h | EC(85), IT ^c (15) | 1101.94 [49.0] 1107.92 [22.3] | ${}^{181}\text{Ta}({}^7\text{Li}, 5n)$ | 31.4 |
| ${}^{180m}\text{Hf}$ (8^-) | 5.5 h | IT(99.69), β^- (0.31) | 215.42 [81.6] 332.27 [94] | ${}^{181}\text{Ta}({}^7\text{Li}, x)$ | |
| ${}^{183}\text{Ta}$ ($7/2^+$) | 5.1 d | β^- (100) | 443.16 [81.7] 246.05 [27.2] 353.98 [11.6] | ${}^{181}\text{Ta}({}^7\text{Li}, x)$ | |

^a E_{th} represents threshold energy.

^bEC represents electron capture.

^cIT represents isomeric transition.

angular distribution of evaporated particles is monitored at every stage of deexcitation. The yrast parameter is chosen as unity. PACE4 does not account for the preequilibrium (PEQ) emissions during the equilibration process.

B. ALICE14

ALICE14, an updated version of ALICE91, utilizes the Weisskopf-Ewing (WE) model [53] for equilibrium (EQ) process, hybrid Monte-Carlo simulation (HMS) model for PEQ decay [54], and the Bohr-Wheeler [55] fission model. It permits selection of different level density options, such as Fermi gas, Kartaria-Ramamurthy, Obninsk and Gilbert-Cameron. In the present case, back-shifted pairing energies with Fermi gas (FG) level density parameter $a = A/9 \text{ MeV}^{-1}$ are selected. In the case of heavy-ion induced reactions, the actual coupling of Fermi energies may be chosen to get better statistics. The angular momentum information which is not a part of Weisskopf-Ewing calculations is estimated by the model of Chadwick and Oblozinsky. The optical model potential is utilized to predict the inverse cross section of the first residuals formed after ejectile emissions and a classical sharp cutoff algorithm model is used to estimate the values in the subroutine. The Myers-Swiiatecki-Lysekil mass formula including the shell correction was used to calculate the Q values and binding energies during the evaporation of particles. The isomeric states are estimated on the basis of the Huizenga-Vandenbosch model [56]. It is limited to using incident energies of around 200 MeV.

C. EMPIRE3.2.2

EMPIRE3.2.2 is the latest version of the EMPIRE nuclear reaction code and it takes into account three stages of nuclear reaction mechanisms: EQ, PEQ, and direct (DIR) processes. In this work, a full-featured Hauser-Feshbach model including γ cascade is adopted to describe the compound nucleus reaction mechanism [57]. A simplified coupled channel calculation (CCFUS) was used to obtain the reaction cross section for heavy-ion fusion. The PEQ emissions were predicted using the exciton model (EM), which uses 1.5 as the mean free path parameter. Cluster emission based on the Iwamoto-Harada model and width fluctuation with the HRTW (Hofmann,

Richert, Tepel, and Weidenmueller) model up to 3 MeV were selected, and discrete levels were chosen from the RIPL-3 library [58,59]. The nuclear level densities such as Gilbert-Cameron (GC) [60], generalized superfluid model (GSM) [61], and enhanced generalized superfluid model (EGSM) [62] with HF calculations were parametrized for proper representation of the case being considered. Input functions such as optical model parameters, level densities, nuclear masses, fission barriers, and γ -ray strength functions are internally adopted by RIPL-3. In the GC model, the three relevant asymptotic value of a -parameter (\tilde{a}) available in EMPIRE are

$$\text{Ignatyuk } et al.: \tilde{a} = 0.154A + (6.3 \times 10^{-5})A^2 \text{ and } \bar{\gamma} = -0.054,$$

$$\text{Arthur: } \tilde{a} = 0.1375A - (8.36 \times 10^{-5})A^2 \text{ and } \bar{\gamma} = -0.054,$$

$$\text{Iljinov } et al.: \tilde{a} = 0.114A + (9.80 \times 10^{-2})A^{2/3} \text{ and } \bar{\gamma} = -0.051,$$

where a is the level density parameter and $\bar{\gamma}$ denotes the shell effects damping factor. In the present case, we have selected the result of Iljinov *et al.*, which offers comparatively better fit to the result.

IV. RESULTS AND DISCUSSION

A. Production of residues

A quantitative measurement of all the residues populated in the ${}^7\text{Li}$ -induced reaction on ${}^{\text{nat}}\text{Ta}$ was performed within the 4–6.5 MeV/nucleon range. A typical γ -ray spectrum of the 35.3 MeV ${}^7\text{Li}$ irradiated ${}^{\text{nat}}\text{Ta}$ foil collected after 47 min of the EOB is depicted in Fig. 1. It confirms the production of ${}^{183g+m}\text{Os}$, ${}^{183}\text{Ta}$, and ${}^{180m}\text{Hf}$ in the target matrix. The residual cross sections have been compared with the theoretical model calculations, which used Weisskopf-Ewing (WE) model and HF models to estimate the EQ process and the HMS and exciton models for the PEQ process, and are shown in Figs. 2, 3, 5 and 6, respectively. The experimental data are shown by symbols with uncertainty and theoretical estimates are shown by curves. The possible contributing reactions and threshold energies of the evaporated residues are given in Table I. The experimental cross sections of the residual radionuclides are reported in Table II.

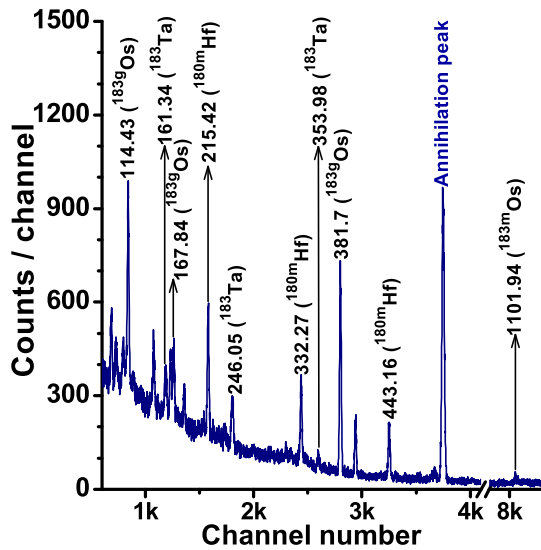


FIG. 1. A γ -ray spectrum of the 35.3 MeV ${}^7\text{Li}$ activated Ta-foil collected after 47 min of the EOB, characteristics γ -ray peaks are shown in keV.

Figure 2 compares the measured cross sections of ${}^{183}\text{gOs}$ along with those reported by Ismail *et al.* [48] and the nuclear model calculations within 30–55 MeV energy. It is observed that the theoretical estimate of ALICE14 overpredicts the reported cross section in Ref. [48]. The newly measured cross sections are found to be $\sim 40\%$ less compared to the previous measurement [48]; however, our experimental results are well reproduced by EMPIRE with GC level density, like other heavy-ion induced reactions such as ${}^7\text{Li} + {}^{93}\text{Nb}/{}^{\text{nat}}\text{Mo}$ and ${}^{11}\text{B} + {}^{89}\text{Y}/{}^{93}\text{Nb}$ [20,21,42,50], which assure the reliability of the model calculations. Nonetheless, ALICE14 and PACE4 estimations do not follow the trend of our cross-section data,

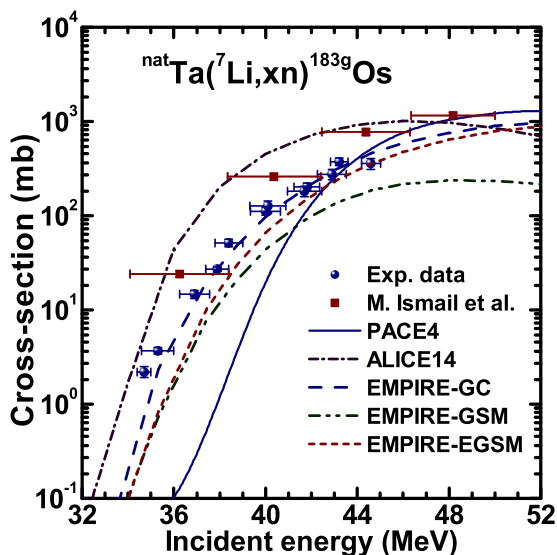


FIG. 2. Comparison of the experimental cross-sections of ${}^{183}\text{gOs}$ with the theoretical estimations from PACE4, ALICE14, and EMPIRE3.2.2 with different level density parameters.

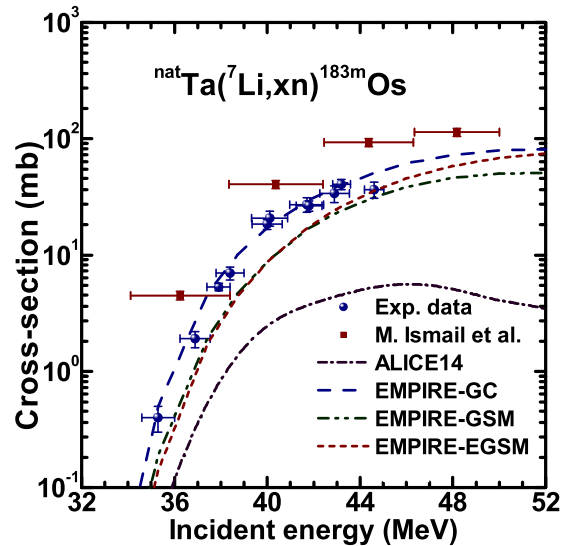


FIG. 3. Comparison of the experimental cross-sections of ${}^{183}\text{mOs}$ with the theoretical estimations from ALICE14 and EMPIRE3.2.2 with different level density models.

showing large overprediction and underprediction, respectively. The measured cross-section of ${}^{183}\text{gOs}$ is also slightly underestimated by the EMPIRE calculation with GSM and EGSM level densities throughout the energy range.

A comparison of experimental and theoretical cross sections of ${}^{183}\text{mOs}$ is depicted in Fig. 3. Similar to the previous case, measured data are in good agreement with the EMPIRE calculations with GC, but are underestimated using the GSM/EGSM level densities. The experimental data follow a similar trend in both metastable and ground state excitation functions with the EMPIRE estimations. ALICE14 largely underestimates the measured cross sections.

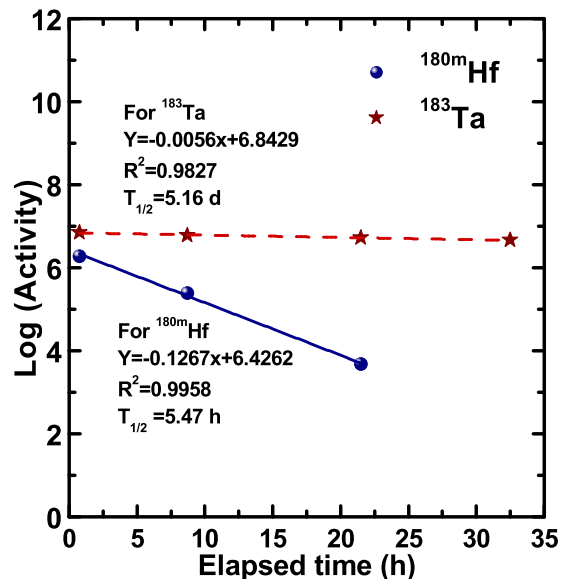


FIG. 4. Half-life estimations for ${}^{180}\text{mHf}$ and ${}^{183}\text{Ta}$.

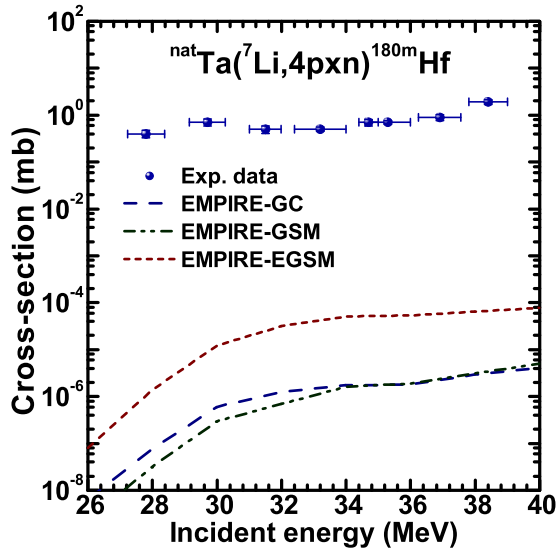


FIG. 5. Comparison of the experimental cross-sections of ${}^{180\text{m}}\text{Hf}$ with EMPIRE3.2.2 with different level density models.

Production of two new radionuclides ${}^{180\text{m}}\text{Hf}$ and ${}^{183}\text{Ta}$ are confirmed in this experiment, although their productions were small compared to other residues. The radionuclides were confirmed from their characteristic γ peaks and decay profiles. The measured half-lives (shown in Fig. 4) of ${}^{180\text{m}}\text{Hf}$ and ${}^{183}\text{Ta}$ are 5.47 h and 5.16 d, respectively, which closely reproduce their actual half-lives. The measured production cross sections of ${}^{180\text{m}}\text{Hf}$ and ${}^{183}\text{Ta}$ are largely underestimated by the nuclear model calculations, as shown in Figs. 5 and 6, respectively. The total cross section of ${}^{180\text{m}}\text{Hf}$ and ${}^{183}\text{Ta}$ estimated from the HF formalism with GC/GSM/EGSM level densities for EQ and EM for PEQ underestimates the experimental data by a factor of $\sim 10^4$ – 10^5 . The enhancement observed in the experimental cross sections essentially indicates the occurrence of the third variety of reaction process,

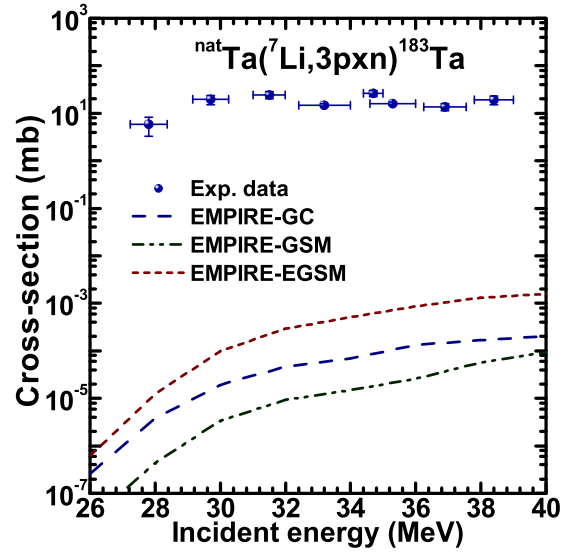


FIG. 6. Same as in Fig. 5 for ${}^{183}\text{Ta}$

which is not considered in the model calculation. It might be due to breakup fusion and transfer followed by breakup-fusion-like processes, generally called partial fusion or ICF, which are probable in the reactions induced by weakly bound projectiles. Several experimental studies have demonstrated a fair possibility of the direct breakup of the weakly bound ${}^7\text{Li}$; the breakup of ${}^6\text{Li}$ and ${}^8\text{Be}$ into $\alpha + d$ and $\alpha + \alpha$ after a nucleon transfer process between the ${}^7\text{Li}$ and target within ~ 3 – 7 MeV/nucleon energy range. The experimental evidence of breakup-fusion and transfer phenomena for weakly bound ${}^7\text{Li}$ projectile is reported in Refs. [23,32,33,63–67].

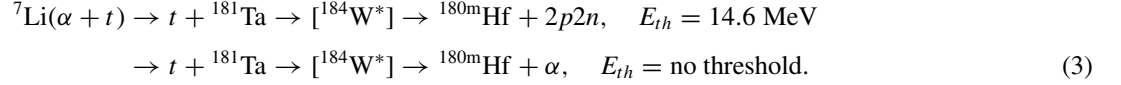
Interaction of ${}^7\text{Li}$ with ${}^{\text{nat}}\text{Ta}$ may lead to the dissociation of ${}^7\text{Li}$ into an α particle and a tritium nucleus (t) in the nuclear force field due to its low breakup threshold [10]. Thus, breakup of the ${}^7\text{Li}$ projectile may essentially lead to the fusion of the t or α particle into the ${}^{\text{nat}}\text{Ta}$ target, which

TABLE II. Experimental cross sections (mb) of the residues at different incident energies.

| Energy (MeV) | Cross section (mb) | | | |
|-----------------|-----------------------------|-----------------------------|-----------------------------|---------------------|
| | ${}^{183\text{g}}\text{Os}$ | ${}^{183\text{m}}\text{Os}$ | ${}^{180\text{m}}\text{Hf}$ | ${}^{183}\text{Ta}$ |
| 27.8 ± 0.6 | | | 0.4 ± 0.07 | 5.8 ± 2.5 |
| 29.7 ± 0.5 | | | 0.7 ± 0.12 | 19.6 ± 4.4 |
| 31.5 ± 0.5 | | | 0.5 ± 0.09 | 24.5 ± 4.4 |
| 33.2 ± 0.8 | | | 0.5 ± 0.05 | 14.9 ± 1.2 |
| 34.7 ± 0.3 | 2.2 ± 0.3 | | 0.7 ± 0.11 | 26.1 ± 3.6 |
| 35.3 ± 0.7 | 3.7 ± 0.3 | 0.4 ± 0.1 | 0.7 ± 0.06 | 15.9 ± 1.3 |
| 36.9 ± 0.6 | 14.7 ± 1.4 | 1.9 ± 0.3 | 0.9 ± 0.13 | 13.6 ± 2.4 |
| 37.9 ± 0.5 | 27.1 ± 1.5 | 5.3 ± 0.4 | | |
| 38.4 ± 0.6 | 51.7 ± 5.0 | 7.0 ± 0.9 | 1.9 ± 0.23 | 19.1 ± 3.8 |
| 40.0 ± 0.6 | 111.9 ± 11.1 | 18.4 ± 1.9 | | |
| 40.1 ± 0.8 | 127.8 ± 16.3 | 20.8 ± 3.1 | | |
| 41.7 ± 0.7 | 182.8 ± 23.1 | 27.2 ± 3.9 | | |
| 41.8 ± 0.5 | 203.5 ± 19.3 | 26.5 ± 2.8 | | |
| 42.9 ± 0.6 | 275.1 ± 34.6 | 33.8 ± 5.6 | | |
| 43.2 ± 0.4 | 374.1 ± 35.4 | 40.5 ± 4.2 | | |
| 44.6 ± 0.4 | 358.2 ± 47.0 | 36.5 ± 5.6 | | |

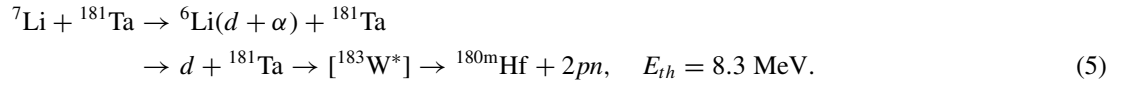
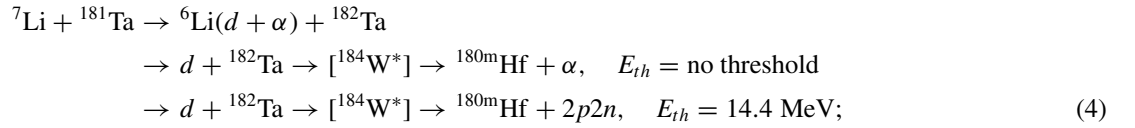
would form the compound nucleus in an excited state, from which emission of nucleons or α particles would lead to the production of $^{180\text{m}}\text{Hf}$ and ^{183}Ta . The possible reaction routes are discussed below.

Fusion of t , a direct breakup component of ^7Li , in ^{181}Ta leads to the formation of excited $^{184}\text{W}^*$, which may emit $2p2n$ or an α particle to form a $^{180\text{m}}\text{Hf}$, while the non-fused α particle flies away in the forward direction:



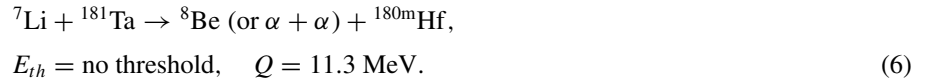
Similarly, fusion of the α component of the dissociated ^7Li with ^{181}Ta would produce an excited composite nucleus ($^{185}\text{Re}^*$), emission of $3p2n$ or αp may lead to $^{180\text{m}}\text{Hf}$, and the t moves in the forward direction; however, this possibility is excluded due to the higher value of threshold energy (35.4 MeV) for the $3p2n$ channel, and the αp emission without n is less probable, although the reaction threshold is 6.08 MeV.

It is also possible that one neutron is stripped off from ^7Li to ^{181}Ta and the projectile, ^6Li , breaks into d and an α particle in the nuclear force field. The fusion of the d component with ^{182}Ta leads to the formation of an excited $^{184}\text{W}^*$ which may emit α or $2p2n$ to produce $^{180\text{m}}\text{Hf}$; while fusion of d in ^{181}Ta would form $^{183}\text{W}^*$ which may emit $2pn$ to form $^{180\text{m}}\text{Hf}$:



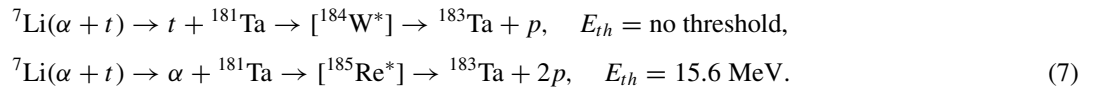
On the other hand, absorption of an α particle by ^{182}Ta would produce $^{180\text{m}}\text{Hf}$ through the $3p3n$ channel; however, this possibility is avoided due to the larger threshold energy 41.2 MeV.

Similarly, a p pickup by ^7Li from ^{181}Ta , would lead to the formation of $^{180\text{m}}\text{Hf}$, and the newly formed ^8Be or its dissociation into two α particles may lead to the following:

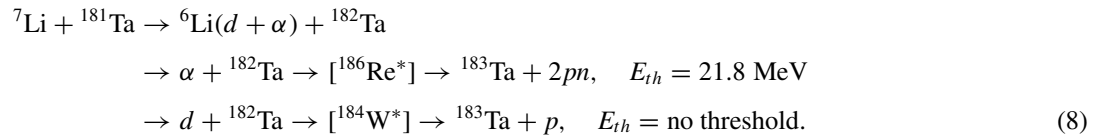


The enhancement ($\sim 10^4$) in the cross section of ^{183}Ta as observed from Fig. 6 compared to the EMPIRE estimations, which mainly considers the direct fusion of the ^7Li projectile into ^{181}Ta , may be understood in the following way.

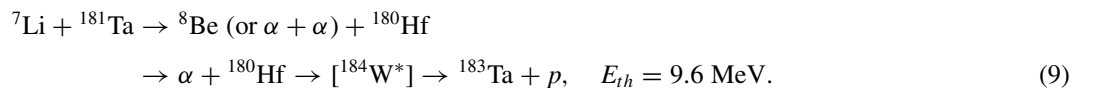
The ^7Li projectile may dissolve into $\alpha + t$, and one of the fragments may fuse to Ta target to form ^{183}Ta through an appropriate channel (p or $2p$), as shown here:



The neutron stripping process may also result to the formation of ^{183}Ta through the following:



Similarly, a p -pickup process would lead to the following:



Fusion of an α particle with ^{181}Ta would follow Eq. (7) in both stripping and pickup of nucleons.

From the analysis of residual cross sections, indirect evidence of ICF for weakly bound projectiles was reported by several groups, including our earlier study for the $^7\text{Li} + ^{93}\text{Nb}$ and $^7\text{Li} + ^{\text{nat}}\text{Mo}$ system [21,38,42]

However, the trend of experimental data is well reproduced by the theory throughout the energy range.

B. Isomeric cross-section ratio (ICR)

If both ground and isomeric states of a nucleus are populated in a reaction, the ratio of cross-sections of those states

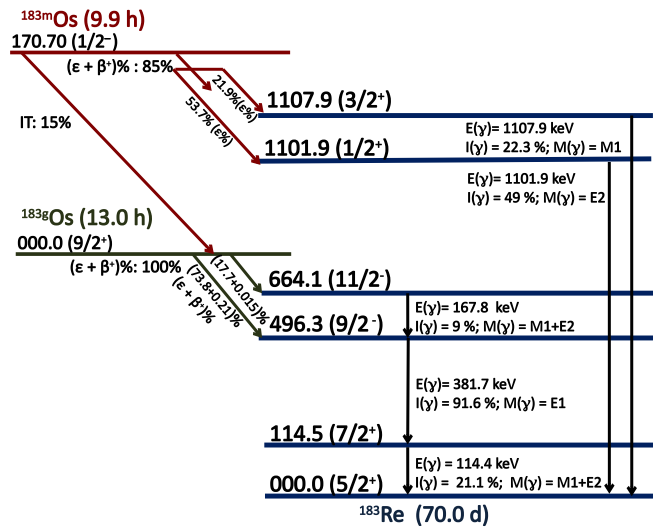


FIG. 7. Abridged decay scheme of ${}^{183\text{g,m}}\text{Os}$ residues with energy levels marked in keV.

is termed ICR. An investigation of ICR provides information about the changes in angular momentum and γ deexcitation processes during the nuclear decay processes. The value of ICR is regulated by several factors such as the energy of the projectile, spin of the target nucleus, type of particle emission, and, more importantly, spin associated with the isomeric state. In this case, ICR is defined as the ratio of cross sections of the low-spin ($\sigma_L \equiv \sigma_m$) to the high-spin ($\sigma_H \equiv \sigma_g$) products. The ground state spin of ${}^{183}\text{Os}$ is 9/2⁺ while the isomeric state ${}^{183\text{m}}\text{Os}$ has the spin of 1/2⁻. The associated decay scheme and the isomeric cross-section ratio of ${}^{183}\text{Os}$ are shown in Figs. 7 and 8, respectively. The experimental ICR data are compared with the estimations of the Hauser-Feshbach formalism with GC/GSM/EGSM against increasing projectile energy. The

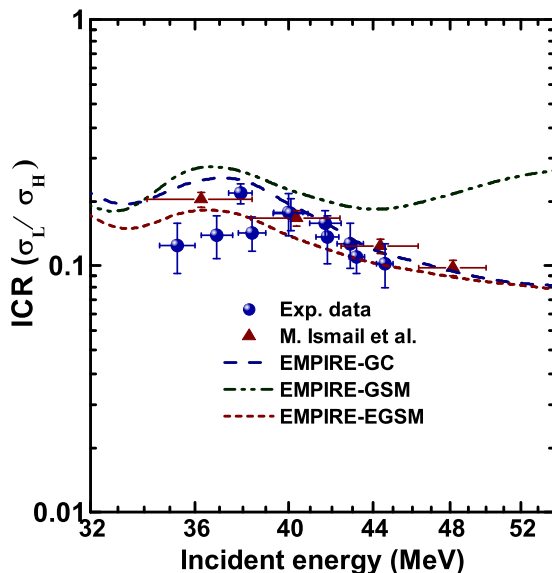


FIG. 8. Comparison of experimental ICR values of ${}^{183}\text{Os}$ with the theoretical estimations from EMPIRE3.2.2.

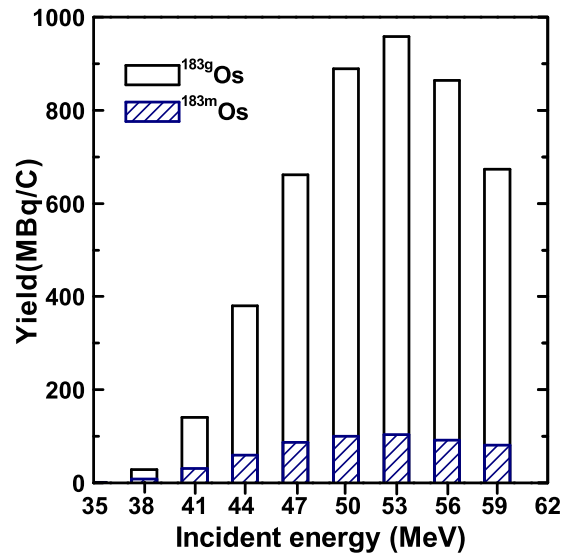


FIG. 9. Production yield of ${}^{183\text{g+m}}\text{Os}$ at distinct bombarding energies.

ICR initially increases sharply due to the enrichment of the low-spin state of 1/2⁻ spin; however, with the increase in excitation energy of the nucleus, population of the high-spin state (9/2⁺) that is the ground state of ${}^{183}\text{Os}$ increases. Therefore, with the rise in incident energy, the value of ICR is decreasing, which indicates the strong tendency of compound nuclear reactions to produce the residual nucleus in higher spin states in the continuum [68]. The experimental ICR agrees well with the HF estimation with GC level density and follows the trend of [48].

C. Yield estimation

Since the theoretical estimation of EMPIRE with GC level density reproduces the experimental cross-sections satisfactorily, it could be used to estimate the production yields of ${}^{183\text{g}}\text{Os}$ and ${}^{183\text{m}}\text{Os}$ at different energies as reported in Fig. 9. The yield of ${}^{183\text{g}}\text{Os}$ dominates as compared to ${}^{183\text{m}}\text{Os}$ and other coproduced radionuclides. The maximum yields of ${}^{183\text{g}}\text{Os}$ and ${}^{183\text{m}}\text{Os}$ are estimated as ~ 960 MBq/C and ~ 100 MBq/C, respectively, at 53 MeV incident energy, where a uniform experimental target thickness of 3.3 mg/cm² is chosen. It is important to note that the yield data are sensitive to beam current (μA) and irradiation time (h), which are taken as unity in the present case. A cumulative yield, commonly known as thick target yield (T_Y), of a residue could be measured if the beam is effectively paused within the target or significantly deteriorated near the threshold energy for the product concerned. Physical T_Y values for ${}^{183\text{g}}\text{Os}$ and ${}^{183\text{m}}\text{Os}$ are deduced using the estimated cross sections of the radioisotopes and stopping power of ${}^7\text{Li}$ in ${}^{\text{nat}}\text{Ta}$ over the range from threshold to 53 MeV energy, where the maximum production of the radioisotopes was observed, using the relation

$$T_Y = \frac{G_t N_A \lambda_r}{M Z e} \int_{E_0}^{E_i} \frac{\sigma_r(E)}{\left(\frac{\delta E}{\delta X}\right)} dE, \quad (10)$$

where $\sigma_r(E)$ is the estimated cross-section from EMPIRE, $(\delta E/\delta X)$ is the stopping power of the target ($\text{MeV g}^{-1}\text{cm}^2$), and E_i and E_0 are the incident projectile energy and energy of the projectile at which the reaction cross section of the residue becomes zero, respectively. G_r is the isotopic enrichment of the target, N_A is Avogadro's number, λ_r (h^{-1}) is the decay constant of the radioisotope, M is the atomic mass of the target, Z is the atomic number of the projectile, and e is the electronic charge. The T_Y values of $^{183\text{g}}\text{Os}$ and $^{183\text{m}}\text{Os}$, to cover the range from threshold to maximum 53 MeV, are estimated as ~ 3530 MBq/C and ~ 423 MBq/C for 87.1 ± 1.5 mg/cm² thick $^{\text{nat}}\text{Ta}$. It is important to note that the reported T_Y of $^{183\text{g+m}}\text{Os}$ is calculated assuming the minimum contamination of impurities within the energy region of interest.

V. SUMMARY

In this article, the production cross sections of $^{183\text{g+m}}\text{Os}$ from the $^7\text{Li} + ^{\text{nat}}\text{Ta}$ reaction have been reported within the energy range 27-45 MeV and are analyzed by comparing with the theoretical model calculations based on the HF and WE models with a suitable set of parameters. The HF formalism

with a coupled channel calculation for the determination of fusion cross section reproduces the measured data fairly well compared to the WE model, which largely overpredicts the data. It is understood that the compound reaction mechanism is the decisive route for the production of $^{183\text{g,m}}\text{Os}$ residues. The small cross sections of $^{180\text{m}}\text{Hf}$ and ^{183}Ta observed in the reaction indicate the occurrence of breakup/transfer followed by fusion or ICF process in the $^7\text{Li} + ^{\text{nat}}\text{Ta}$ reaction at relatively low energy. The trend of ICR describes the effect of angular momentum and spin distribution, and hence the formation of isomers. The maximum production yield of $^{183\text{g,m}}\text{Os}$ is found at ~ 53 MeV, which would help to fix the required energy window for the optimum production of $^{183\text{g,m}}\text{Os}$.

ACKNOWLEDGMENTS

We sincerely thank Prof. S. Lahiri, SINP, Kolkata, for his generous support during the experiment, and Pelletron and target laboratory staff of the BARC-TIFR Pelletron facility for their cooperation and help during the experiment. Support through a fellowship from MHRD, Government of India, is gratefully acknowledged by A.C.

-
- [1] L. F. Canto, P. R. S. Gomes, R. Donangelo, and M. S. Hussein, *Phys. Rep.* **424**, 1 (2006).
- [2] A. Diaz-Torres, I. J. Thompson, and C. Beck, *Phys. Rev. C* **68**, 044607 (2003).
- [3] P. K. Rath, S. Santra, N. L. Singh, B. K. Nayak, K. Mahata, R. Palit, K. Ramachandran, S. K. Pandit, A. Parihari, A. Pal, S. Appannababu, S. K. Sharma, D. Patel, and S. Kailas, *Phys. Rev. C* **88**, 044617 (2013).
- [4] H. Esbensen, *Phys. Rev. C* **81**, 034606 (2010).
- [5] M. Ray, A. Mukherjee, M. K. Pradhan, R. Kshetri, M. S. Sarkar, R. Palit, I. Majumdar, P. K. Joshi, H. C. Jain, and B. Dasmahapatra, *Phys. Rev. C* **78**, 064617 (2008).
- [6] H. Freiesleben, H. C. Britt, J. Birkelund, and J. R. Huizenga, *Phys. Rev. C* **10**, 245 (1974).
- [7] N. Keeley, R. Raabe, N. Alamanos, and J. L. Sida, *Prog. Part. Nucl. Phys.* **59**, 579 (2007).
- [8] N. Keeley, N. Alamanos, K. W. Kemper, and K. Rusek, *Prog. Part. Nucl. Phys.* **63**, 396 (2009).
- [9] A. Pakou, N. Keeley, D. Pierroutsakou, M. Mazzocco, L. Acosta, X. Aslanoglou, A. Boiano, C. Boiano, D. Carbone, M. Cavallaro, J. Grebosz, M. La Commara, C. Manea, G. Marquinez-Duran, I. Martel, C. Parascandolo, K. Rusek, A. M. Sanchez-Benitez, O. Sgouros, C. Signorini, F. Soramel, V. Soukeras, E. Stiliaris, E. Strano, D. Torresi, A. Trzcinska, Y. X. Watanabe, and H. Yamaguchi, *Eur. Phys. J. A* **51**, 90 (2015).
- [10] A. Pakou, O. Sgouros, V. Soukeras, F. Cappuzzello, N. Keeley, L. Acosta, C. Agodi, X. Aslanoglou, S. Calabrese, D. Carbone, M. Cavallaro, A. Foti, G. Marquinez-Duran, I. Martel, M. Mazzocco, C. Parascandolo, D. Pierroutsakou, K. Rusek, E. Strano, V. A. B. Zagatto, and K. Zerva, *Phys. Rev. C* **95**, 044615 (2017).
- [11] V. Soukeras, A. Pakou, F. Cappuzzello, L. Acosta, C. Agodi, N. Alamanos, S. Calabrese, D. Carbone, M. Cavallaro, A. Cunsolo, A. Di Pietro, J. P. Fernández-García, P. Figuera, M. Fisichella, A. Foti, N. Keeley, G. Marquinez-Duran, I. Martel, M. Mazzocco, D. Pierroutsakou, K. Rusek, G. Santagati, O. Sgouros, E. Stiliaris, E. Strano, D. Torresi, and K. Zerva, *Phys. Rev. C* **95**, 054614 (2017).
- [12] O. Sgouros, A. Pakou, D. Pierroutsakou, M. Mazzocco, L. Acosta, X. Aslanoglou, C. Betsou, A. Boiano, C. Boiano, D. Carbone, M. Cavallaro, J. Grebosz, N. Keeley, M. La Commara, C. Manea, G. Marquinez-Duran, I. Martel, N. G. Nicolis, C. Parascandolo, K. Rusek, A. M. Sanchez-Benitez, C. Signorini, F. Soramel, V. Soukeras, C. Stefanini, E. Stiliaris, E. Strano, I. Strojek, and D. Torresi, *Phys. Rev. C* **95**, 054609 (2017).
- [13] C. Beck, N. Rowley, P. Papka, S. Courtin, M. Rousseau, F. A. Souza, N. Carlin, F. Liguori Neto, M. M. De Moura, M. G. Del Santo, A. A. I. Suade, M. G. Munhoz, E. M. Szanto, A. Szanto De Toledo, N. Keeley, A. Diaz-Torres, and K. Hagino, *Int. J. Mod. Phys. E* **20**, 943 (2011).
- [14] C. Beck, N. Rowley, P. Papka, S. Courtin, M. Rousseau, F. A. Souza, N. Carlin, R. Liguori Neto, M. M. de Moura, M. G. Del Santo, A. A. P. Suaide, M. G. Munhoz, E. M. Szanto, A. Szanto de Toledo, N. Keeley, A. Diaz-Torres, and K. Hagino, *Nucl. Phys. A* **834**, 440c (2010).
- [15] F. A. Souza, N. Carlin, C. Beck, N. Keeley, A. Diaz-Torres, R. Liguori Neto, C. Siqueira-Mello, M. M. de Moura, M. G. Munhoz, R. A. N. Oliveira, M. G. Del Santo, A. A. P. Suaide, E. M. Szanto, and A. Szanto de Toledo, *Nucl. Phys. A* **834**, 420c (2010).
- [16] P. R. S. Gomes, J. Lubian, L. F. Canto, D. R. Otomar, D. R. Mendes, Jr., P. N. de Faria, R. Linares, L. Sigaud, J. Rangel, J. L. Ferreira, E. Ferioli, B. Paes, E. N. Cardozo, M. R. Cortes, M. J. Ermamatov, P. Lotti, and M. S. Hussein, *Few-Body Syst.* **57**, 165 (2016).
- [17] N. N. Deshmukh, S. Mukherjee, B. K. Nayak, D. C. Biswas, S. Santra, E. T. Mirgule, S. Appannababu, D. Patel, A. Saxena,

- R. K. Choudhury, J. Lubian, and P. R. S. Gomes, *Eur. Phys. J. A* **47**, 118 (2011).
- [18] J. M. Figueira, J. O. Fernández Niello, D. Abriola, A. Arazi, O. A. Capurro, E. de Barbará, G. V. Martí, D. Martínez Heimann, A. E. Negri, A. J. Pacheco, I. Padrón, P. R. S. Gomes, J. Lubian, T. Correa, and B. Paes, *Phys. Rev. C* **75**, 017602 (2007).
- [19] A. Di Pietro, P. Figuera, E. Strano, M. Fisichella, O. Goryunov, M. Lattuada, C. Maiolino, C. Marchetta, M. Milin, A. Musumarra, V. Ostashko, M. G. Pellegriti, V. Privitera, G. Randisi, L. Romano, D. Santonocito, V. Scuderi, D. Torresi, and M. Zadro, *Phys. Rev. C* **87**, 064614 (2013).
- [20] D. Kumar, M. Maiti, and S. Lahiri, *Phys. Rev. C* **94**, 044603 (2016).
- [21] D. Kumar and M. Maiti, *Phys. Rev. C* **96**, 044624 (2017).
- [22] M. Dasgupta, P. R. S. Gomes, D. J. Hinde, S. B. Moraes, R. M. Anjos, A. C. Berriman, R. D. Butt, N. Carlin, J. Lubian, C. R. Morton, J. O. Newton, and A. Szanto de Toledo, *Phys. Rev. C* **70**, 024606 (2004).
- [23] H. Kumawat, V. Jha, V. V. Parkar, B. J. Roy, S. K. Pandit, R. Palit, P. K. Rath, C. S. Palshetkar, S. K. Sharma, S. Thakur, A. K. Mohanty, A. Chatterjee, and S. Kailas, *Phys. Rev. C* **86**, 024607 (2012).
- [24] A. M. M. Maciel, P. R. S. Gomes, J. Lubian, R. M. Anjos, R. Cabezas, G. M. Santos, C. Muri, S. B. Moraes, R. Liguori Neto, N. Added, N. Carlin Filho, and C. Tenreiro, *Phys. Rev. C* **59**, 2103 (1999).
- [25] K. Zerva, A. Pakou, N. Patronis, P. Figuera, A. Musumarra, A. Di Pietro, M. Fisichella, T. Glodariu, M. La Commara, M. Lattuada, M. Mazzocco, M. G. Pellegriti, D. Pierroutsakou, A. M. Sanchez-Benitez, V. Scuderi, E. Strano, and K. Rusek, *Eur. Phys. J. A* **48**, 102 (2012).
- [26] C. S. Palshetkar, S. Thakur, V. Nanal, A. Shrivastava, N. Dokania, V. Singh, V. V. Parkar, P. C. Rout, R. Palit, R. G. Pillay, S. Bhattacharyya, A. Chatterjee, S. Santra, K. Ramachandran, and N. L. Singh, *Phys. Rev. C* **89**, 024607 (2014).
- [27] A. Pakou, N. Alamanos, A. Lagoyannis, A. Gillibert, E. C. Pollacco, P. A. Assimakopoulos, G. Doukelis, K. G. Ioannides, D. Karadimos, D. Karamanis, M. Kokkoris, E. Kossionides, N. G. Nicolis, C. Papachristodoulou, N. Patronis, G. Perdikakis, and D. Pierroutsakou, *Phys. Lett. B* **556**, 21 (2003).
- [28] A. Pakou, N. Alamanos, G. Doukelis, A. Gillibert, G. Kalyva, M. Kokkoris, S. Kossionides, A. Lagoyannis, A. Musumarra, C. Papachristodoulou, N. Patronis, G. Perdikakis, D. Pierroutsakou, E. C. Pollacco, and K. Rusek, *Phys. Rev. C* **69**, 054602 (2004).
- [29] K. Zerva, A. Pakou, K. Rusek, N. Patronis, N. Alamanos, X. Aslanoglou, D. Filipescu, T. Glodariu, N. Keeley, M. Kokkoris, M. La Commara, A. Lagoyannis, M. Mazzocco, N. G. Nicolis, D. Pierroutsakou, and M. Romoli, *Phys. Rev. C* **82**, 044607 (2010).
- [30] R. Raabe, C. Angulo, J. L. Charvet, C. Jouanne, L. Nalpas, P. Figuera, D. Pierroutsakou, M. Romoli, and J. L. Sida, *Phys. Rev. C* **74**, 044606 (2006).
- [31] O. Sgouros, A. Pakou, D. Pierroutsakou, M. Mazzocco, L. Acosta, X. Aslanoglou, C. Betsou, A. Boiano, C. Boiano, D. Carbone, M. Cavallaro, J. Grebosz, N. Keeley, M. La Commara, C. Manea, G. Marquez-Duran, I. Martel, N. G. Nicolis, C. Parascandolo, K. Rusek, A. M. Sanchez-Benitez, C. Signorini, F. Soramel, V. Soukeras, C. Stefanini, E. Stiliaris, E. Strano, I. Strojek, and D. Torresi, *Phys. Rev. C* **94**, 044623 (2016).
- [32] S. K. Pandit, A. Shrivastava, K. Mahata, N. Keeley, V. V. Parkar, P. C. Rout, K. Ramachandran, I. Martel, C. S. Palshetkar, A. Kumar, A. Chatterjee, and S. Kailas, *Phys. Rev. C* **93**, 061602(R) (2016).
- [33] D. Chattopadhyay, S. Santra, A. Pal, A. Kundu, K. Ramachandran, R. Tripathi, B. J. Roy, T. N. Nag, Y. Sawant, B. K. Nayak, A. Saxena, and S. Kailas, *Phys. Rev. C* **97**, 051601(R) (2018).
- [34] L. F. Canto, P. R. S. Gomes, J. Lubian, L. C. Chamon, and E. Crema, *Nucl. Phys. A* **821**, 51 (2009).
- [35] L. F. Canto, D. R. Mendes, Jr., P. R. S. Gomes, and J. Lubian, *Phys. Rev. C* **92**, 014626 (2015).
- [36] Z. H. Liu, C. Signorini, M. Mazzocco, M. Ruan, H. Q. Zhang, T. Glodariu, Y. W. Wu, F. Soramel, C. J. Lin, and F. Yang, *Eur. Phys. J. A* **26**, 73 (2005).
- [37] P. R. S. Gomes, M. D. Rodriguez, G. V. Marti, I. Padron, L. C. Chamon, J. O. Fernandez Niello, O. A. Capurro, A. J. Pacheco, J. E. Testoni, A. Arazi, M. Ramirez, R. M. Anjos, J. Lubian, R. Veiga, R. Liguori Neto, E. Crema, N. Added, C. Tenreiro, and M. S. Hussein, *Phys. Rev. C* **71**, 034608 (2005).
- [38] N. T. Zhang, Y. D. Fang, P. R. S. Gomes, J. Lubian, M. L. Liu, X. H. Zhou, G. S. Li, J. G. Wang, S. Guo, Y. H. Qiang, Y. H. Zhang, D. R. Mendes, Jr., Y. Zheng, X. G. Lei, B. S. Gao, Z. G. Wang, K. L. Wang, and X. F. He, *Phys. Rev. C* **90**, 024621 (2014).
- [39] V. V. Parkar, V. Jha, S. K. Pandit, S. Santra, and S. Kailas, *Phys. Rev. C* **87**, 034602 (2013).
- [40] O. A. Capurro, D. E. DiGregorio, S. Gil, D. Abriola, M. di Tada, J. O. Fernandez Niello, A. O. Macchiavelli, G. V. Marti, A. J. Pacheco, J. E. Testoni, D. Tomasi, and I. Urteaga, *Phys. Rev. C* **53**, 1301 (1996).
- [41] D. H. Luong, M. Dasgupta, D. J. Hinde, R. du Rietz, R. Rafiei, C. J. Lin, M. Evers, and A. Diaz-Torres, *Phys. Rev. C* **88**, 034609 (2013).
- [42] D. Kumar and M. Maiti, *Phys. Rev. C* **96**, 014617 (2017).
- [43] M. Maiti and S. Lahiri, *Phys. Rev. C* **81**, 024603 (2010).
- [44] M. Maiti, *Phys. Rev. C* **84**, 044615 (2011).
- [45] M. Maiti and S. Lahiri, *Phys. Rev. C* **79**, 024611 (2009).
- [46] M. Maiti and S. Lahiri, *Phys. Rev. C* **84**, 067601 (2011).
- [47] J. S. Foster, J. W. Hilborn, and L. Yaffe, *Can. J. Phys.* **36**, 555 (1958).
- [48] M. Ismail, R. P. Sharma, and M. H. Rashid, *Phys. Rev. C* **57**, 1290 (1998).
- [49] J. F. Ziegler, *J. Appl. Phys.* **85**, 1249 (1999).
- [50] D. Kumar and M. Maiti, *Phys. Rev. C* **95**, 064602 (2017).
- [51] A. Gavron, *Phys. Rev. C* **21**, 230 (1980).
- [52] O. B. Tarasov and D. Bazin, *Nucl. Instrum. Methods B* **266**, 4657 (2008).
- [53] V. F. Weisskopf and D. H. Ewing, *Phys. Rev.* **57**, 472 (1940).
- [54] M. Blann, *Phys. Rev. C* **54**, 1341 (1996).
- [55] N. Bohr and J. A. Wheeler, *Phys. Rev.* **56**, 426 (1939).
- [56] R. Vandenbosch and J. R. Huizenga, *Phys. Rev.* **120**, 1313 (1960).
- [57] H. Feshbach, A. Kerman, and S. Koonin, *Ann. Phys. (NY)* **125**, 429 (1980).
- [58] E. Betak and J. Cseh, *EPJ Web. Conf.* **146**, 12023 (2017).
- [59] R. Capote, M. Herman, P. Obložinsky, P. G. Young, S. Goriely, T. Belgya, A. V. Ignatyuk, A. J. Koning, S. Hilaire, V. A. Plujko,

- M. Avrigeanu, O. Bersillon, M. B. Chadwick, T. Fukahori, Z. Ge, Y. Han, S. Kailas, J. Kopecky, V. M. Maslov, G. Reffo, M. Sin, E. Sh. Soukhovitskii, and P. Talou, *Nucl. Data Sheets* **110**, 3107 (2009).
- [60] A. Gilbert and A. G. W. Cameron, *Can. J. Phys.* **43**, 1446 (1965).
- [61] A. V. Ignatyuk, J. L. Weil, S. Raman, and S. Kahane, *Phys. Rev. C* **47**, 1504 (1993).
- [62] V. A. Plujko, O. M. Gorbachenko, B. M. Bondar, and E. P. Rovenskykh, *Nucl. Data Sheets* **118**, 240 (2014).
- [63] M. Fisichella, A. C. Shotton, P. Figuera, J. Lubian, A. Di Pietro, J. P. Fernandez-Garcia, J. L. Ferreira, M. Lattuada, P. Lotti, A. Musumarra, M. G. Pellegriti, C. Ruiz, V. Scuderi, E. Strano, D. Torresi, and M. Zadro, *Phys. Rev. C* **95**, 034617 (2017).
- [64] V. V. Parkar, S. K. Sharma, R. Palit, S. Upadhyaya, A. Shrivastava, S. K. Pandit, K. Mahata, V. Jha, S. Santra, K. Ramachandran, T. N. Nag, P. K. Rath, B. Kanagalekar, and T. Trivedi, *Phys. Rev. C* **97**, 014607 (2018).
- [65] V. Tripathi, A. Navin, V. Nanal, R. G. Pillay, K. Mahata, K. Ramachandran, A. Shrivastava, A. Chatterjee, and S. Kailas, *Phys. Rev. C* **72**, 017601 (2005).
- [66] A. Shrivastava, A. Navin, N. Keeley, K. Mahata, K. Ramachandran, V. Nanal, V. V. Parkar, A. Chatterjee, and S. Kailas, *Phys. Lett. B* **633**, 463 (2006).
- [67] E. C. Simpson, K. J. Cook, D. H. Luong, S. Kalkal, I. P. Carter, M. Dasgupta, D. J. Hinde, and E. Williams, *Phys. Rev. C* **93**, 024605 (2016).
- [68] K. Kim, G. N. Kim, H. Naik, M. Zaman, S. C. Yang, T. Y. Song, R. Guin, and S. K. Das, *Nucl. Phys. A* **935**, 65 (2015).